Electronic Supplementary Material (ESI) for Journal of Materials Chemistry C.

Electronic Supplementary Information

Luminescence quenching in epitaxially grown PCN-224 type metal-organic frameworks

Tobias Burger,[1] Miriam Velásquez-Hernández,[2] Robert Saf,[3]
Sergey M. Borisov,*[,1] and Christian Slugovc*[,3]

[1] *Graz University of Technology, Institute of Analytical Chemistry and Food Chemistry; Stremayrgasse 9; 8010 Graz; Austria*

[2] *Graz University of Technology, Institute of Physical and Theoretical Chemistry; Stremayrgasse 9; 8010 Graz; Austria*

[3] *Graz University of Technology, Institute for Chemistry and Technology of Materials; Stremayrgasse 9; 8010 Graz; Austria*

**corresponding authors: sergey.borisov@tugraz.at, slugovc@tugraz.at*

Chemicals and Materials

H_2TCPP was obtained from Porphyrin Laboratories (www.porphyrin-laboratories.com, Gleschendorf, Germany). Pt(II)PCN-224 and PCN-224 was prepared as described in literature.[1] *N,N*-dimethylformamide (DMF), zirconyl chloride hydrate ($ZrOCl_2 \cdot 8H_2O$) and acetic acid (HAc) were purchased from Roth (www.carlroth.com). Acetone was acquired from VWR (www.vwr.com) and NH_4HCO_3 was obtained from Sigma Aldrich (www.sigmaaldrich.com). All reagents were used as received.

Optical microscopy images were acquired with an Olympus DSX-1000 instrument with crossed polarizers (as shown in Fig. 1) and in bright field mode (as shown in the ESI) (www.olympus-global.com). UV/Vis spectra were recorded on a Cary50 spectrophotometer from Varian (www.varian.com).

PXRD measurements were done using a Rigaku SmartLab X-Ray Diffractometer (www.rigaku.com) with a 9 kW, Cu anode (λ=1.5406 Å).

SEM images were acquired using a TESCAN MIRA3 microscope. All Samples were deposited on clean silicon wafers and carbon coated before the measurements. EDS measurements were done with Ametek EDAX EDX Super Octane detector.

Acquisition of emission spectra, excitation spectra and oxygen quenching experiments were performed on a Fluorolog-3 luminescence spectrometer from Horiba (www.horiba.com), equipped with a NIR sensitive detector R2658 from Hamamatsu (www.hamamatsu.com). Oxygen partial pressure was adjusted with mass flow controllers from Voegtlin (www.voegtlin.com, Aesch, Switzerland) by mixing either nitrogen and compressed air (for calibration up to 20 kPa partial pressure of oxygen) or 0.2 % oxygen in nitrogen and nitrogen 7.0 (99.99999 % purity) for trace oxygen calibration. Calibration gases were acquired from Linde gas (www.linde-gas.de). A previously described custom-made setup using optical fibers to guide excitation and emission light was used.[2] As sample holder, a standard 6 mm diameter NMR tube was used.

Excitation spectra of the physically mixed MOF and the statistically mixed MOF were recorded in aqueous dispersion placed in a screw-cap cuvette von Hellma. About 0.1 mg MOF powder were dispersed in water and spectra were recorded in air-saturated and anoxic conditions. For the latter, the dispersion was deoxygenated by bubbling argon through for at least 10 minutes. Emission wavelength λ_{em} was 650 nm in all the experiments.

Preparation of physically mixed MOF

0.3 mg PCN-224 obtained according to a reported procedure[3] was mixed with 0.3 mg Pt(II)PCN-224 by dispersing in 1 mL acetone in a 3 mL glass vial. Both MOFs were activated prior to mixing at 120 °C for 24 h. The mixture was transferred into a standard NMR tube (considered as an appropriate vessel for such small amounts of compound). After careful evaporation of the solvent at elevated temperature, the sample was activated again at 120 °C for 72 h.

Preparation of statistically mixed MOF

4 mg Pt(II)TCPP (4 µmol), 3 mg H_2TCPP (4 µmol), 32 $ZrOCl_2 \cdot 8\ H_2O$ (100 µmol) and 6.2 mL HAc were mixed with 12.5 mL DMF. The mixture was sonicated for 20 minutes and placed in an oven at 65 °C for 72h. After cooling to room temperature, crystals were harvested by centrifugation. After washing trice with DMF (3x 3 mL) and acetone (3x 3 mL) and solvent exchange (trice with acetone at 65 °C),

MOFs were activated. For activation, crystals were transferred to an NMR tube and kept under vacuum at 120 °C for 72 h.

Preparation of Core-Shell Mixed MOFs

Pt(II)PCN-224 core/PCN-224 shell MOF

7.7 mg Pt(II)TCPP (7.7 µmol) and 32 mg $ZrOCl_2 \cdot 8\,H_2O$ (100 µmol) were dissolved in the mixture of 6.2 mL HAc and 12.5 mL DMF. After sonication for 20 minutes, the reaction mixture was placed in an oven at 65 °C for one week. After red crystals could be observed under optical light microscope, the reaction mixture was quickly centrifuged. The solution of reactants for the shell MOF was prepared by dissolving 3 mg TCPP and 16 mg $ZrOCl_2 \cdot 8H_2O$ in the mixture of 3.1 mL HAc and 6.25 mL DMF. The centrifuged core-crystals of Pt(II)PCN-224 added to this solution and the mixture was placed again in the oven at 65 °C. Samples at 24, 48 and 72 h (all remaining crystals) were collected, purified and activated in the same was as described for the statistically mixed MOF.

PCN-224 core/Pt(II)PCN-224 shell MOF

Synthesis of the core (PCN-224) was carried out following a previously reported procedure.[2] After around 30 h of synthesis, the core MOF (PCN-224) was obtained by centrifugation. The obtained solid crystals were mixed with fresh precursor solution containing 7.7 mg Pt(II)TCPP and 32.2 mg $ZrOCl_2 \cdot 8H_2O$ in the mixture of 12.5 mL DMF and 6.2 mL HAc that was sonicated for 20 minutes prior to addition of the seed crystals. The reaction mixture was kept in an oven at 65 ° C for another 72 h. Purification and activation of the MOF materials was done as described above for the statistically mixed MOF.

Core/shell MOFs with Pt(II)PCN-224 and Pd(II)PCN-224 were prepared with the same synthesis procedure but 7.7 mg Pt(II)TCPP and 7 mg Pd(II)PCN-224 were used. Time of synthesis was 72h for core materials and 72h for shell materials. Purification and activation was done as described for the other MOFs.

Digestion of MOF materials

The ratio of the two porphyrins was assessed by digesting the MOF and recording UV-VIS spectra of the digested porphyrin solution. Digestion protocol was adapted from a previously reported procedure.[4] In a typical procedure, 1 mg of activated MOF powder was digested in 2 mL aqueous 1M NH_4HCO_3 solution while sonication for 10 minutes at room temperature. The obtained solutions were diluted with DMF to the concentration appropriate for UV-VIS measurements. The ratio of porphyrins was estimated from the absorbance in the maxima of the absorption bands at 402 nm (Pt(II)TCPP) and 418 nm (H_2TCPP) using the molar absorption coefficients of 270.000 L mol^{-1} cm^{-1} and 240.000 L mol^{-1} cm^{-1}, respectively. [5]

Microscopy images of the mixed MOF materials

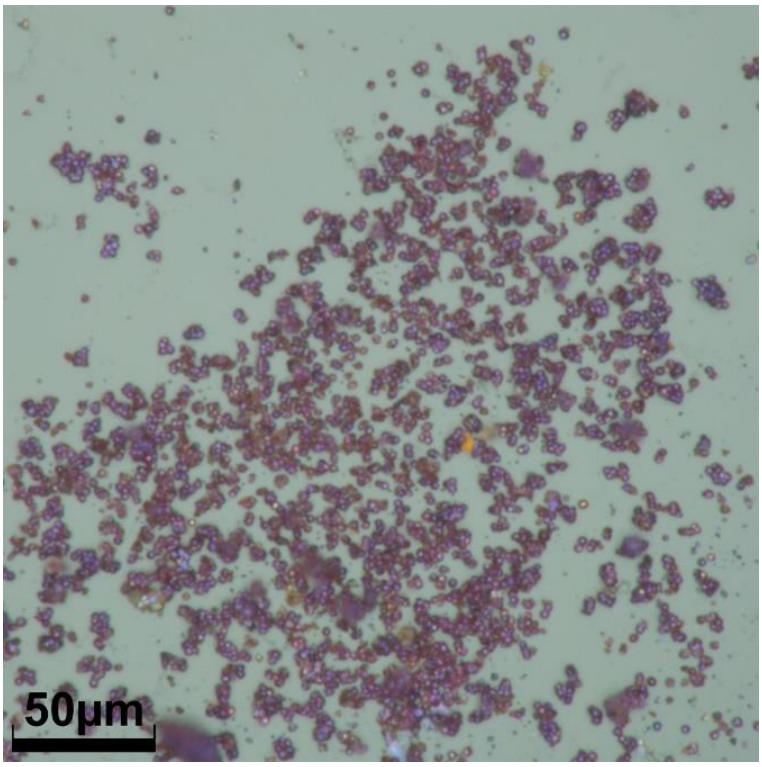

Fig. S1: Optical microscopy image of core-shell MOF with Pt(II)PCN-224 in the core and PCN-224 in the shell. The shell was grown for 24h.

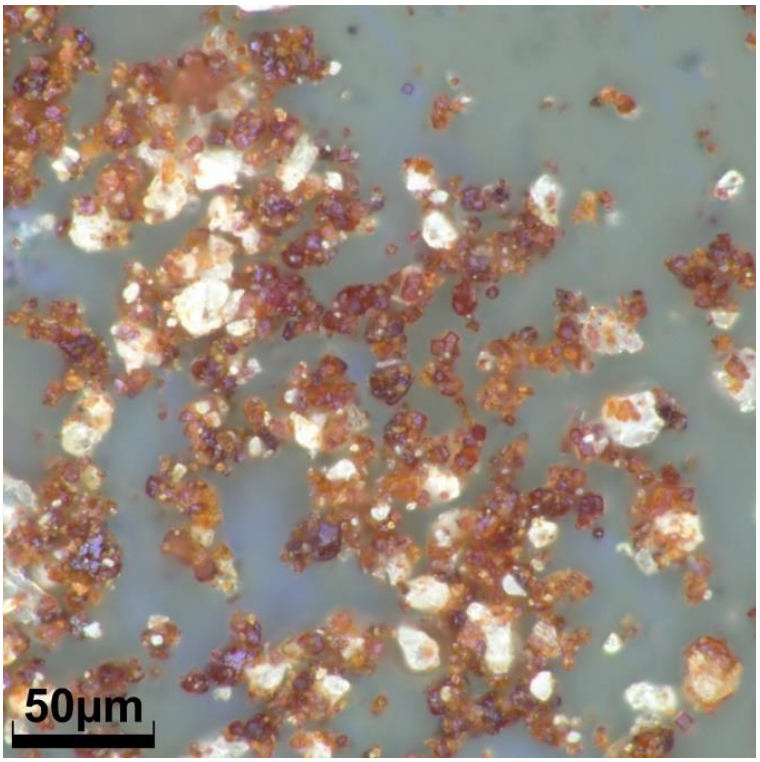

Fig. S2: Optical microscopy image of core-shell MOF with Pt(II)PCN-224 in the core and PCN-224 in the shell. Shell growth was 48 h. A colorless side product can be observed next to the red crystals.

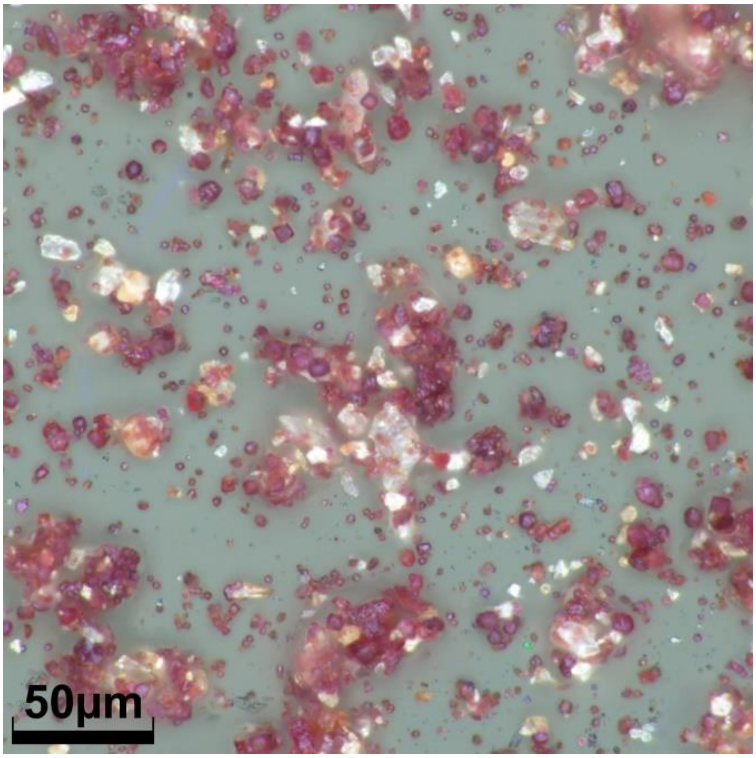

Fig. S3: Optical microscopy image of core-shell MOF with Pt(II)PCN-224 in the core and PCN-224 in the shell after 72h of shell growth.

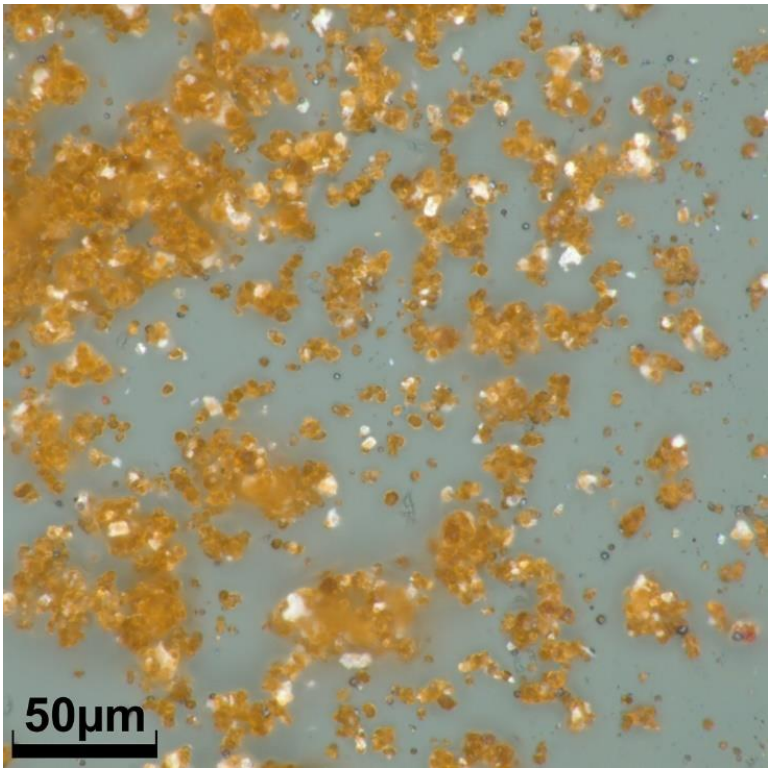

Fig. S4: Optical microscopy image of core-shell MOF with PCN-224 in the core and Pt(II)PCN-224 in the shell.

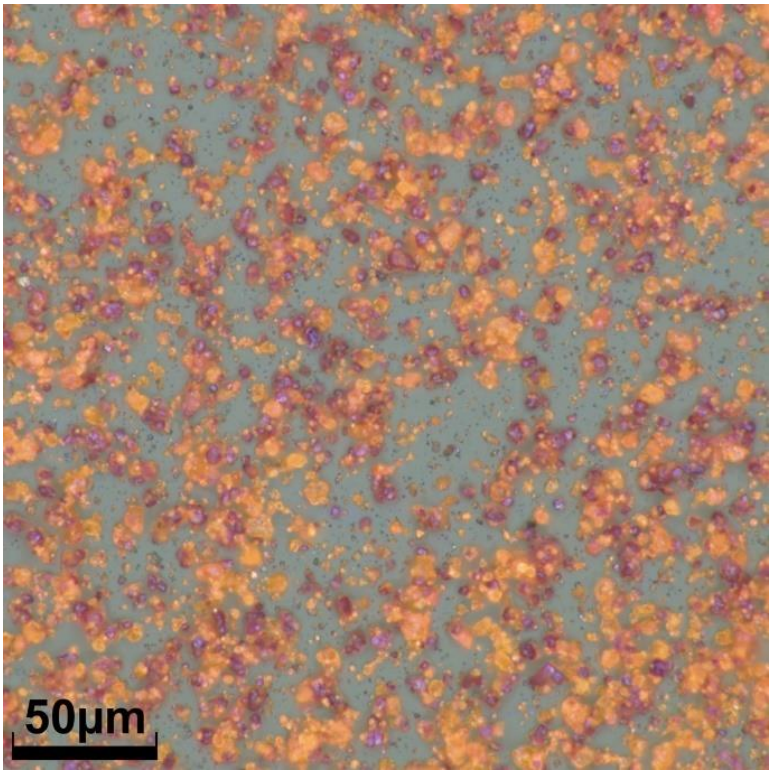

Fig. S5: Optical microscopy image of physically mixed PCN-224 and Pt(II)PCN-224 MOFs.

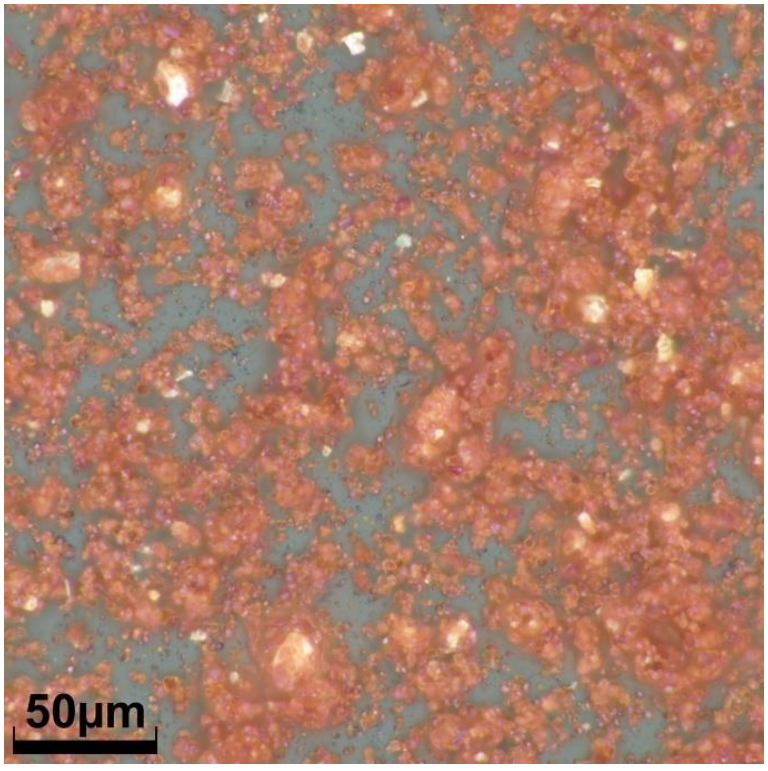

Fig. S6: Optical microscopy image of statistically mixed MOF prepared by co-crystallization of H_2TCPP and Pt(II)TCPP.

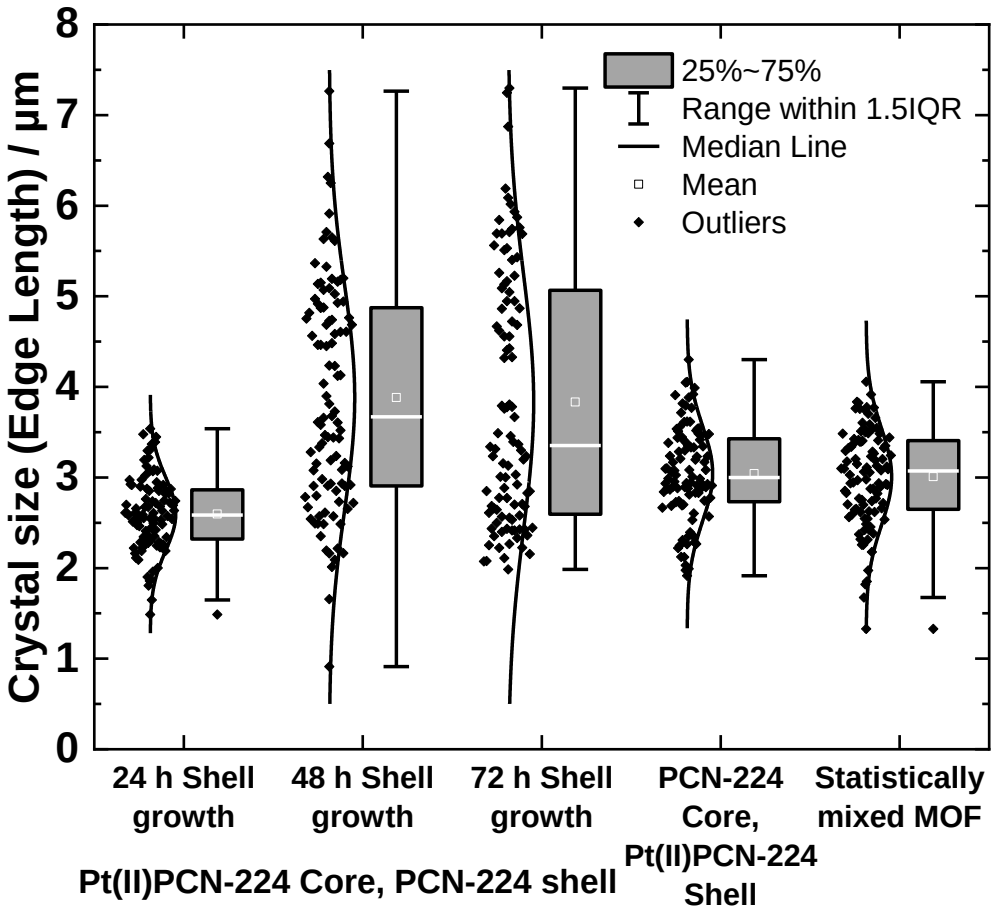

Fig. S7: Particle size of the mixed MOF materials. From each sample at least 100 individual crystals were measured.

Tab. S1: Molar ratios of the mixed MOFs and quenchability expressed as I_0/I.

Material	**Molar ratio Pt(II)PCN-224: PCN-224**	**$I_0/I_{20\ kPa}$ λ_{Ex} = 410 nm**	**$I_0/I_{20\ kPa}$ λ_{Ex} = 500 nm**
Physically mixed MOF	1:0.9	48	
Statistically mixed MOF	1:1.25	5.7	8.5
Pt(II)PCN-224 core PCN-224 shell (24 h shell growth)	1:0.9	2.6	5.6
Pt(II)PCN-224 core PCN-224 shell (48 h shell growth)	1:1.6	3.2	5.1
Pt(II)PCN-224 core PCN-224 shell (72 h shell growth)	1:5	4.5	5.7
PCN-224 core Pt(II)PCN-224 shell	1:0.7	3.6	

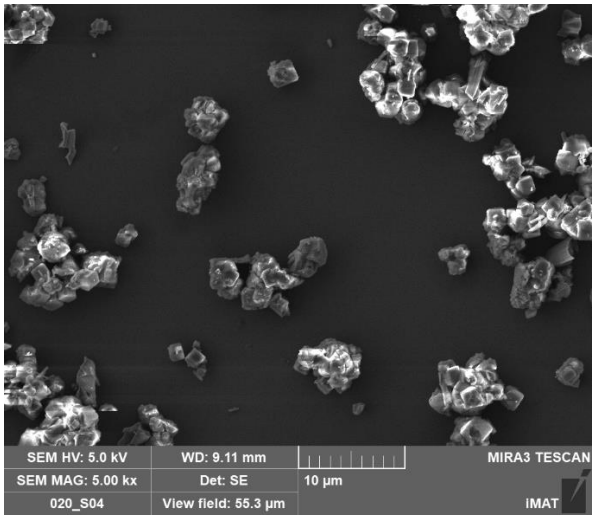

PCN-224 in the core and Pt(II)PCN-224 in shell 24 h

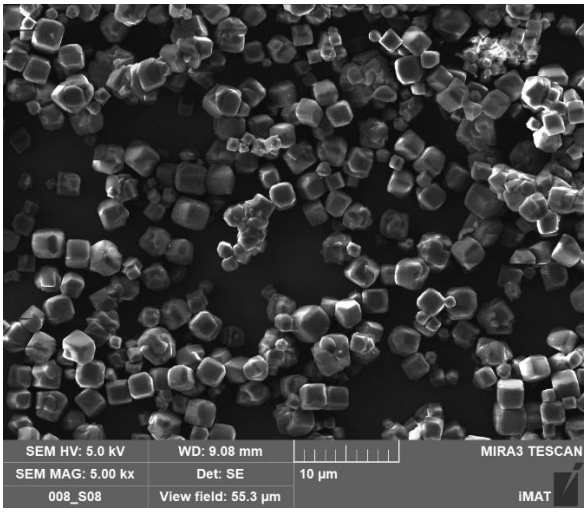

statistically mixed Pt(II)PCN-224 and PCN-224

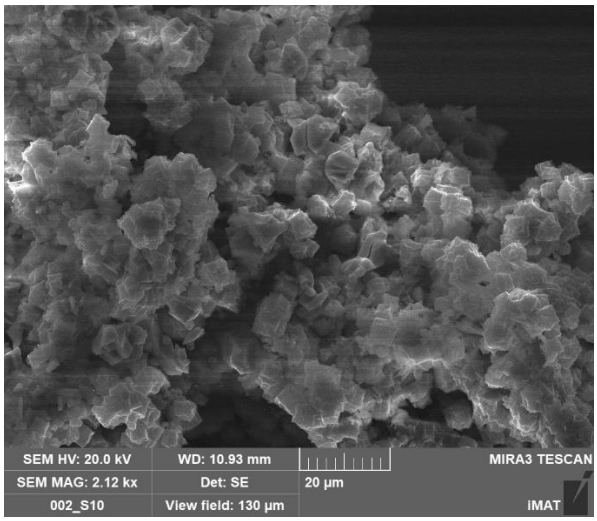

PCN-224 in the core and Pt(II)PCN-224 in shell 48 h

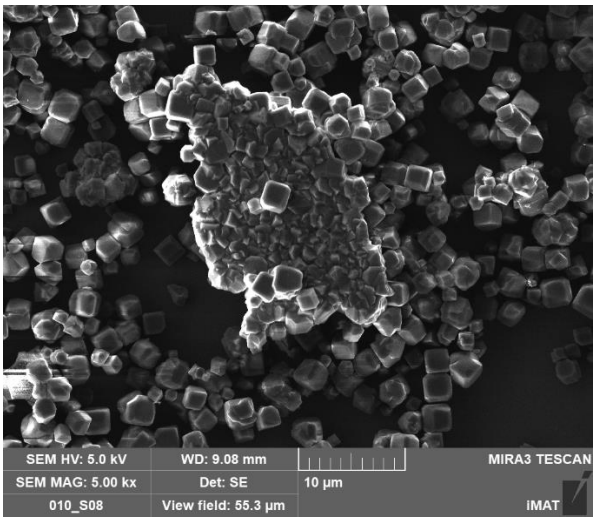

Pt(II)PCN-224 in the core and PCN-224 in shell

Fig. S8. Scanning electron micrographs of the MOFs.

Investigations towards identifying the colorless side product

The nature of the colourless side products visible e.g. in Fig S2 was further studied. pXRD patterns of all samples do not show crystalline non-porous materials (as an example for a potential crystalline side product m-ZrO_2 was recorded).

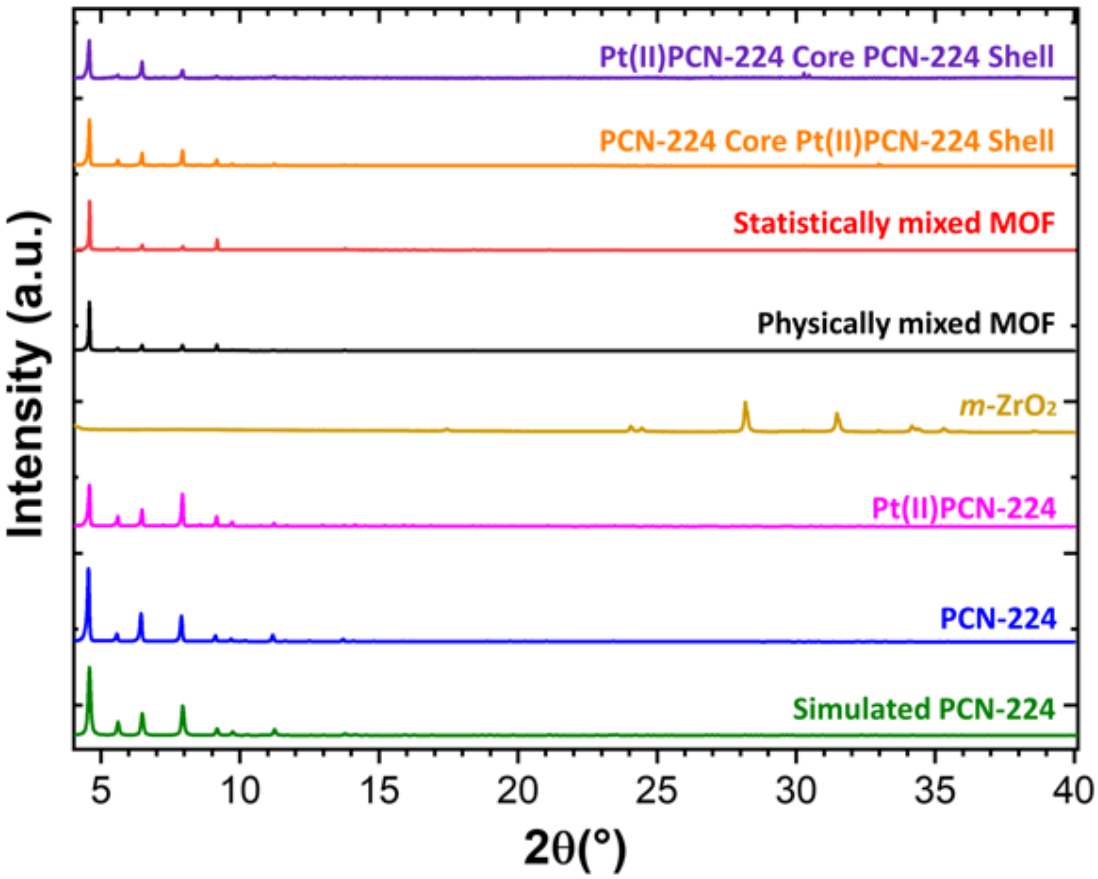

Fig. S9: pXRD-patterns of the samples discussed here including data for m-ZrO2

Further we analysed the colourless side product by using a RAMAN microscope, but could not retrieve information suited to elucidate the nature of the side product. In a next step, we conducted the SEM investigation requested below and recorded EDX of the MOF and the side product.

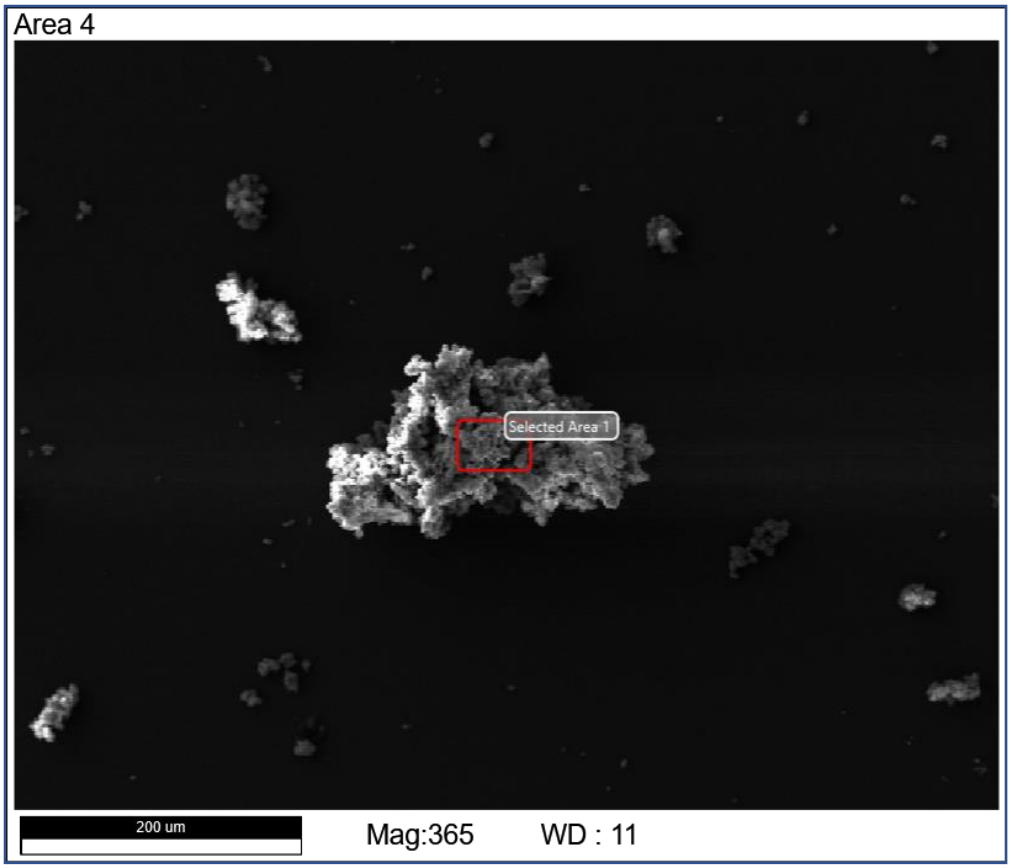

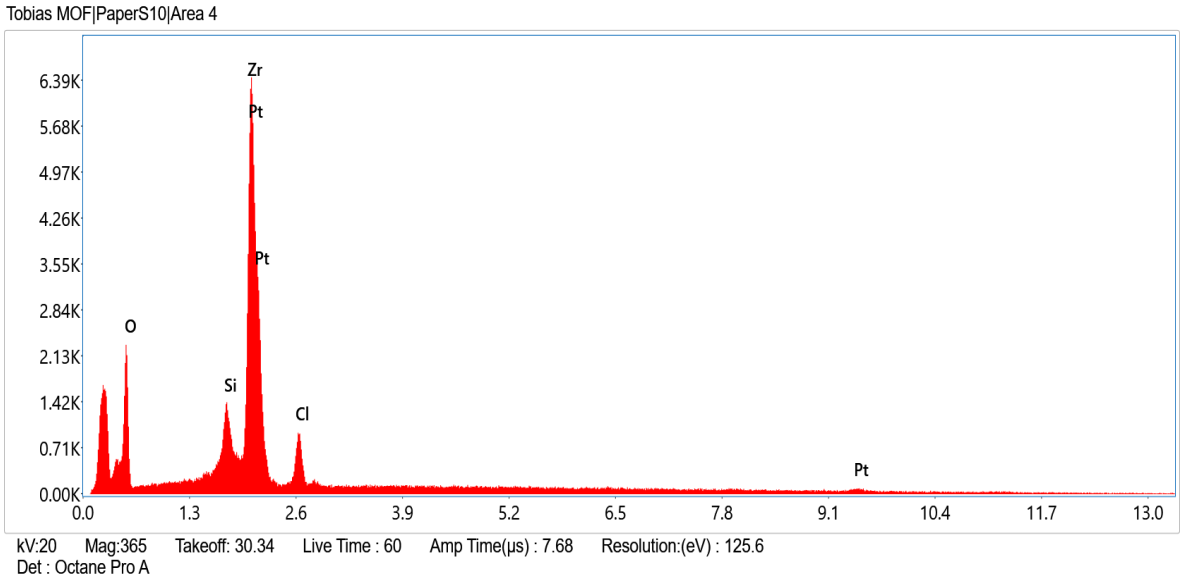

Fig. S10: pXRD SEM image and EDX analysis of core-shell MOF with Pt(II)PCN-224 in core and PCN-224 in the shell after 48h of shell growth (this is the sample where the impurities are most prevalent; below).

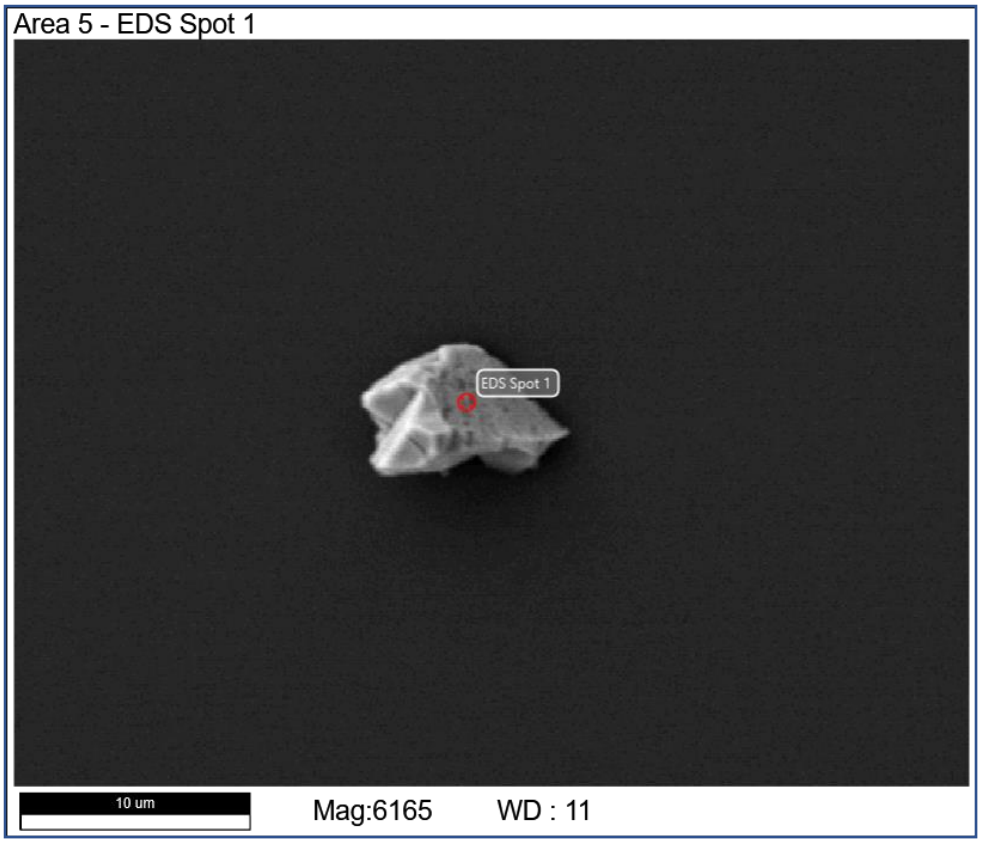

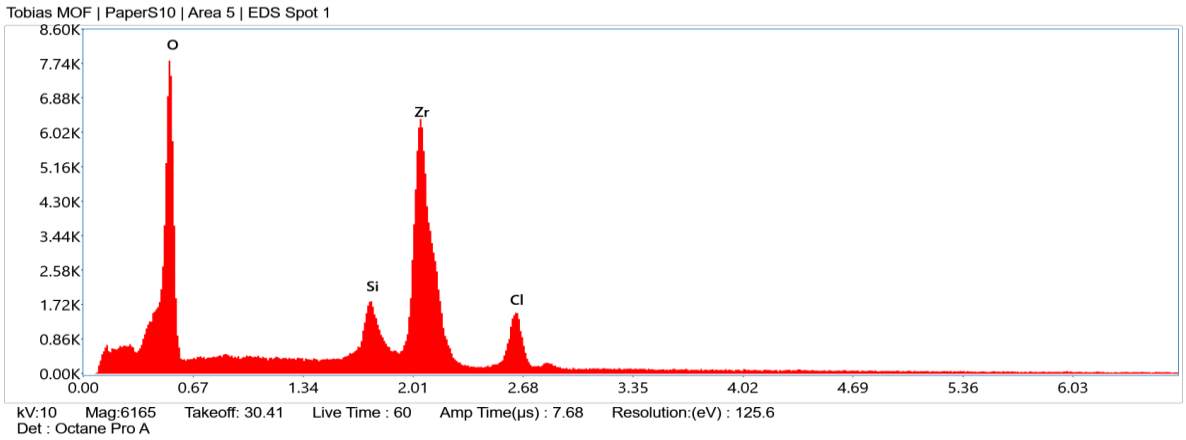

Fig. S11: SEM image of one of the white impurities found in core-shell synthesis (sample Pt(II)PCN-224 in core and PCN-224 in shell, 48h of shell growth) and EDX analysis. Si is from the substrate (silicon wafer).

From these investigations it became clear that the side product is amorphous and contains Zr and most probably O and Cl.

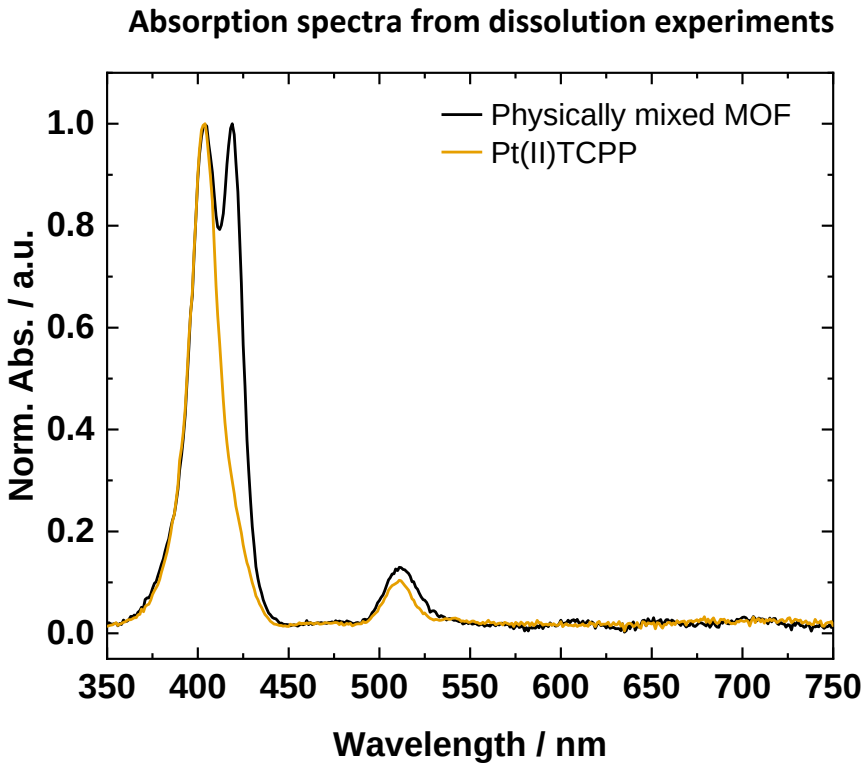

Fig. S12: Absorption spectrum of digested physically mixed PCN-224 and Pt(II)PCN-224 MOF in DMF. For comparison the normalized absorption spectrum of Pt(II)TCPP (digested Pt(II)PCN-224) in DMF is also given. The absorption peak at 420 nm is from H_2TCPP (digested PCN-224).

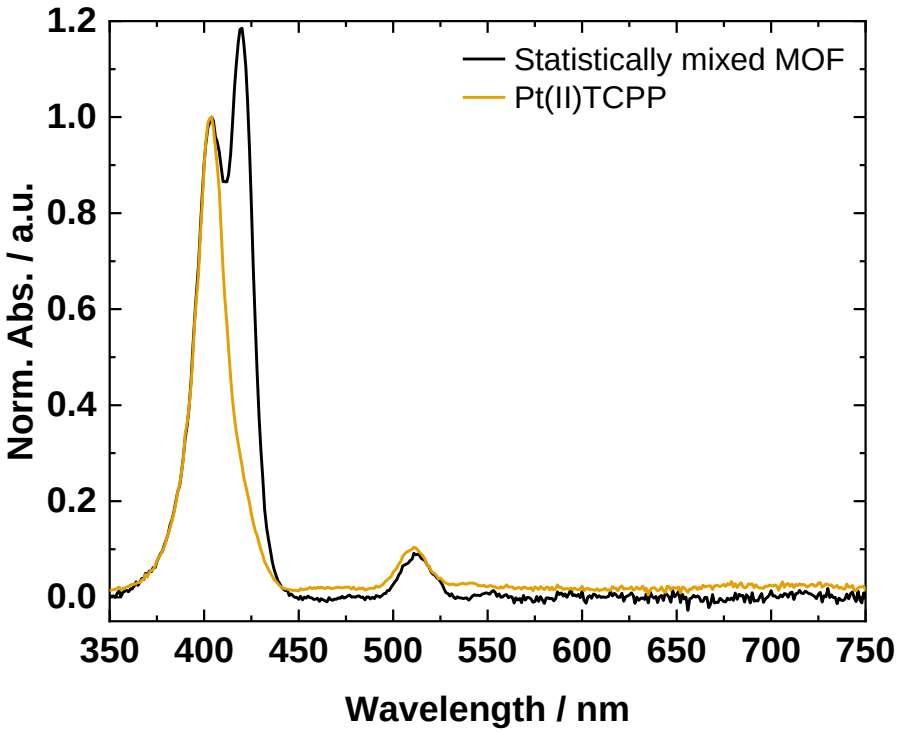

Fig. S13: Absorption spectrum of digested statistically mixed MOF in DMF. For comparison the normalized absorption spectrum of Pt(II)TCPP (digested Pt(II)PCN-224) in DMF is also given.

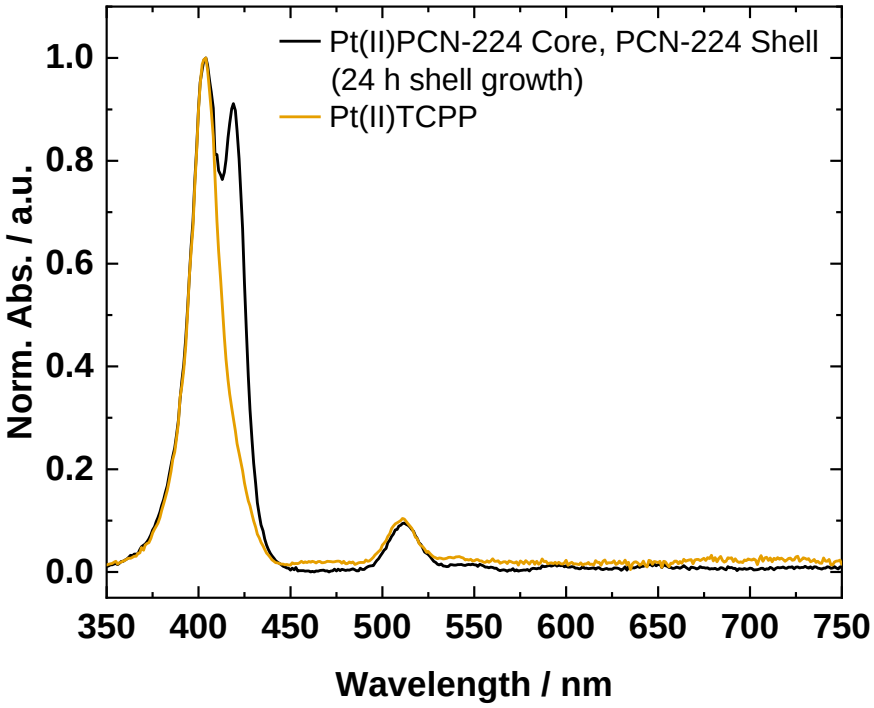

Fig. S14: Absorption spectra of digested core-shell MOF with Pt(II)PCN-224 in the core and PCN-224 in the shell (24 h shell growth) in DMF. For comparison the normalized absorption spectrum of Pt(II)TCPP (digested Pt(II)PCN-224) in DMF is also given.

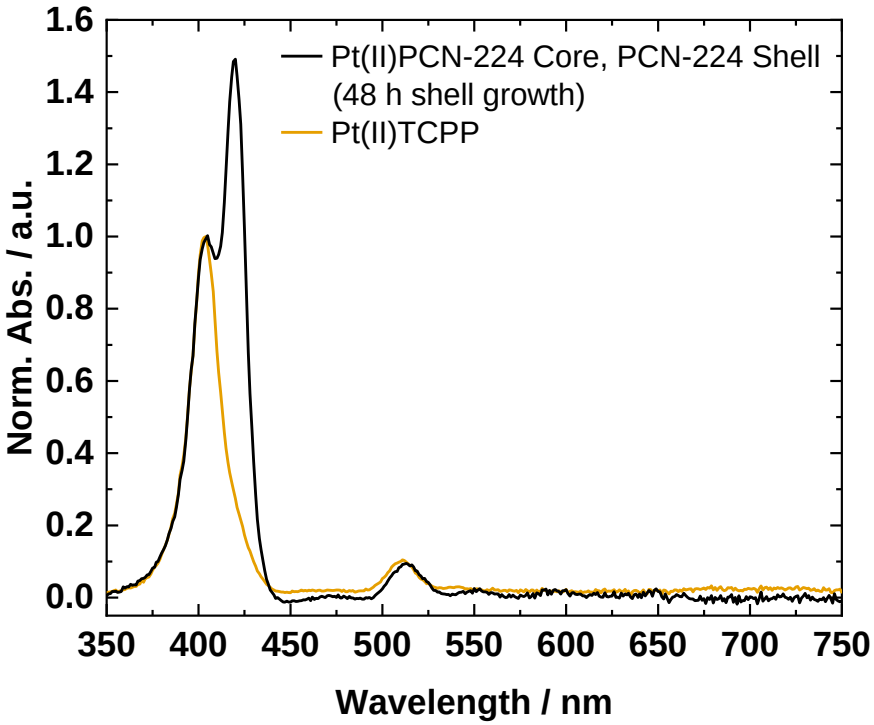

Fig. S15: Absorption spectra of digested core-shell MOF with Pt(II)PCN-224 in the core and PCN-224 in the shell (48 h shell growth) in DMF. For comparison the normalized absorption spectrum of Pt(II)TCPP (digested Pt(II)PCN-224) in DMF is also given.

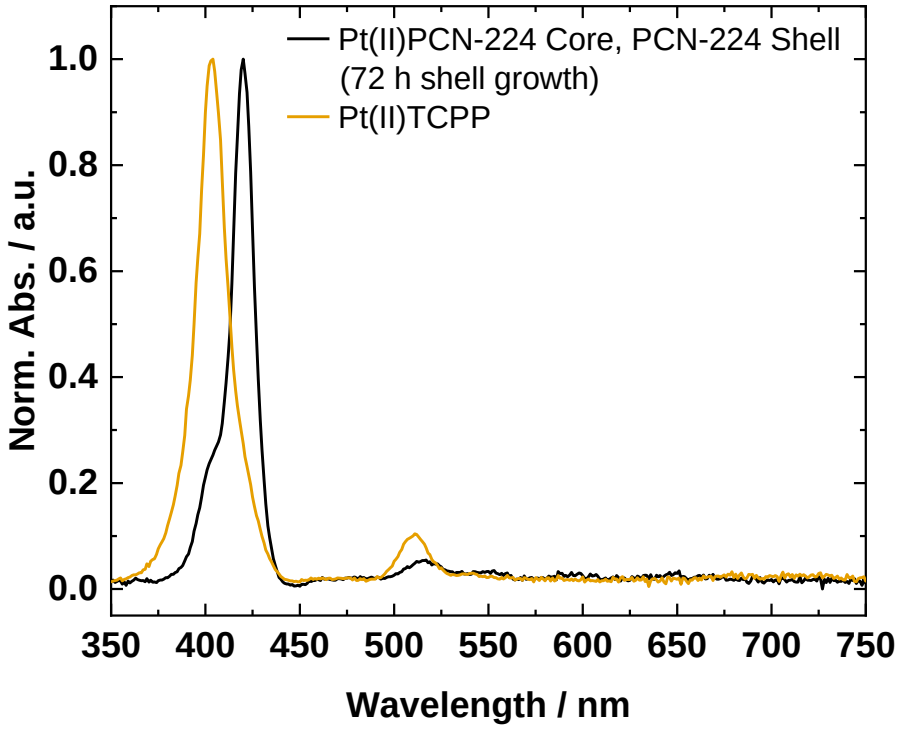

Fig. S16: Absorption spectra of digested core-shell MOF with Pt(II)PCN-224 in core and PCN-224 in shell (72 h shell growth) in DMF. For comparison the normalized absorption spectrum of Pt(II)TCPP (digested Pt(II)PCN-224) in DMF is also given.

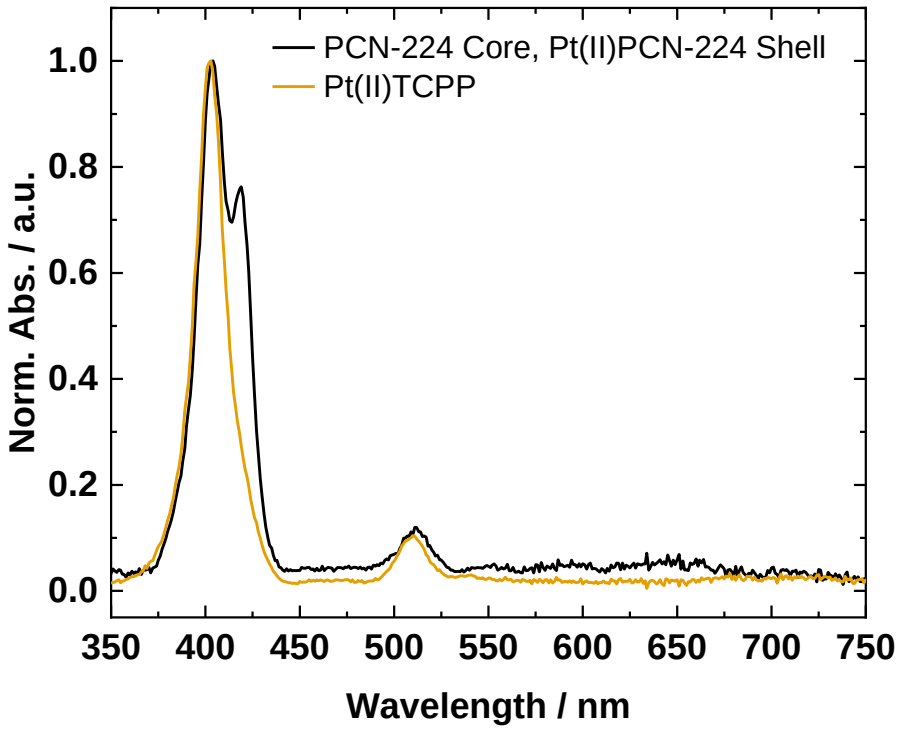

Fig. S17. Absorption spectrum of digested core-shell MOF with PCN-224 in the core and Pt(II)PCN-224 in the shell in DMF. For comparison the normalized absorption spectrum of Pt(II)TCPP (digested Pt(II)PCN-224) in DMF is also given.

Considerations regarding quantification of luminescence quenching by molecular oxygen in the mixed MOF systems

Luminescence quenching in general is described by the Stern-Volmer equation (S1).

$$\frac{I_0}{I_0} = 1 + K_{SV} \cdot [O_2] \qquad \text{(S1)}$$

I_0 is the luminescence intensity under anoxic conditions and I is the intensity at a given oxygen concentration. K_{SV} is the Stern Volmer constant and τ_0 the respective luminescence decay time in oxygen-free atmosphere.

Deviation from linear Stern-Volmer behavior of immobilized luminescent sensing materials is often observed. The non-linearity caused by heterogeneity of the environment has been discussed in literature and the extended Stern-Volmer "two-site model" (eq.S2) [6] proved to be highly useful to describe the non-linear behavior. Non-linearity of quenching in the case of MOFs can have different reasons, such as defects in the MOF, blocking of pores due to encapsulated reactants or solvents, different oxygen accessibility on MOF/air interface and many more. Especially the influence of defects in MOFs is not well understood and of high interest in the MOF community[7–9] . The two-site model (eq. S2) extends the Stern-Volmer model by introducing the second Stern-Volmer constant K_{SV2} corresponding to the quenching of dye in the second environment. Distribution of the indicator between the two environments is expressed by distribution factor f.

$$\frac{I_0}{I} = \frac{1}{\frac{f}{1+K_{SV1} \cdot [O_2]} + \frac{1-f}{1+K_{SV2} \cdot [O_2]}} \qquad \text{(S2)}$$

It was already shown that the two-site model describes the quenching behavior of PCN-224 and related materials very well [2]. Nevertheless, in the case of mixed-MOFs, the two-site model does not always fully describe the quenching behavior since two different materials (PCN-224, Pt(II)PCN-224) with completely different sensitivities are difficult to fit in this equation. Fit parameters for the mixed MOFs obtained with the two-site model are available in Tab. S1. Here, the two-site model was applied for fitting of the trace oxygen region and for fitting the full range. As can be seen, the Stern Volmer constant K_{SV1} is greatly underestimated in the case of full-range fitting.

Therefore, for description of the mixed MOFs, we propose a further extension of the Stern-Volmer equation in the form of a series expansion with four sensitivities (K_{SV1}, K_{SV2}, K_{SV3}, K_{SV4}) and the four different distribution factors (f_1, f_2, f_3, f_4) according to equation S3.

$$\frac{I_0}{I} = \frac{1}{\frac{f_1}{1+K_{SV1} \cdot [O_2]} + \frac{f_2}{1+K_{SV2} \cdot [O_2]} + \frac{f_3}{1+K_{SV3} \cdot [O_2]} + \frac{1-(f_1+f_2+f_3)}{1+K_{SV4} \cdot [O_2]}} \qquad \text{(S3)}$$

With the boundary condition:

$$\sum f_i = 1 \qquad \text{(S4)}$$

It has to be noted that comparison of oxygen sensitivity becomes more difficult when a high number of descriptors for oxygen sensitivity (several K_{SV} and f values). Fitting experimental data with a fit function containing many degrees of freedom as in eq. S.3 is also difficult.

For the whole measurement range from N_2 to 20 kPa for comparison of sensitivity, an effective Stern-Volmer constant K_{SVeff} as shown in eq. S.5 can then be used for the for the "four-site model" to simplify the comparison.

$$K_{SVeff.} = \sum K_{SVi} \cdot f_i \qquad \text{(S5)}$$

Fig. S25 shows the fit obtained from the extended model with four sensitivities. As can be seen in the insert of the fit parameters, fit converged with a one K_{SV} = 0 and the corresponding *f* very close to 0. That means, the fourth term does not contribute to a higher fit quality and can be omitted for simplicity.

Since fitting with the two-site model delivers an insufficient fit quality and the "four-site model" adequately fits the experimental data but has too many fit parameters to be practical, description with three terms (eq. S6) can be a good compromise. As can be seen in Fig. S26 this model also fits the experimental data very well.

$$\frac{I_0}{I} = \frac{1}{\frac{f}{1+K_{SV1}\cdot[O_2]}+\frac{f_2}{1+K_{SV2}\cdot[O_2]}+\frac{1-(f_1+f_2)}{1+K_{SV3}\cdot[O_2]}} \qquad \text{(S6)}$$

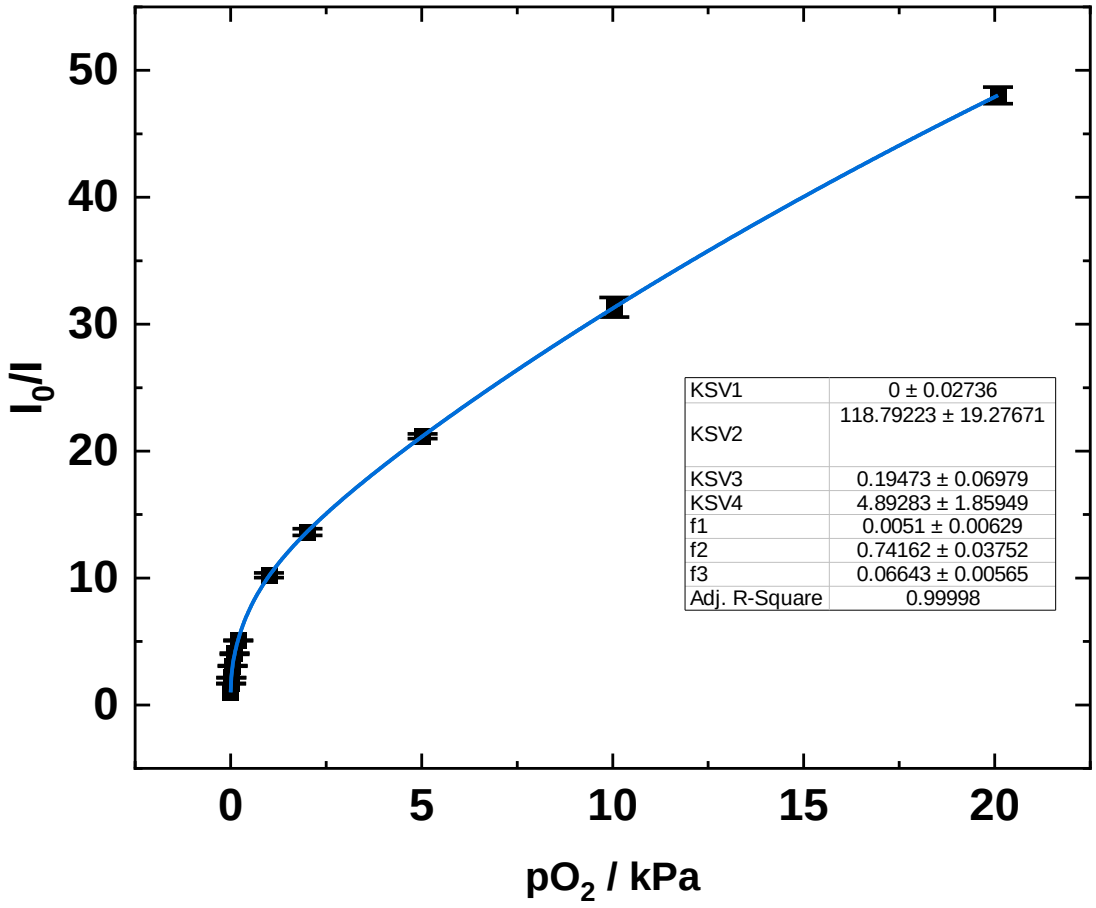

Fig. S18: Stern-Volmer plot of the physically mixed MOF and fit with eq. S3 ("four-site model").

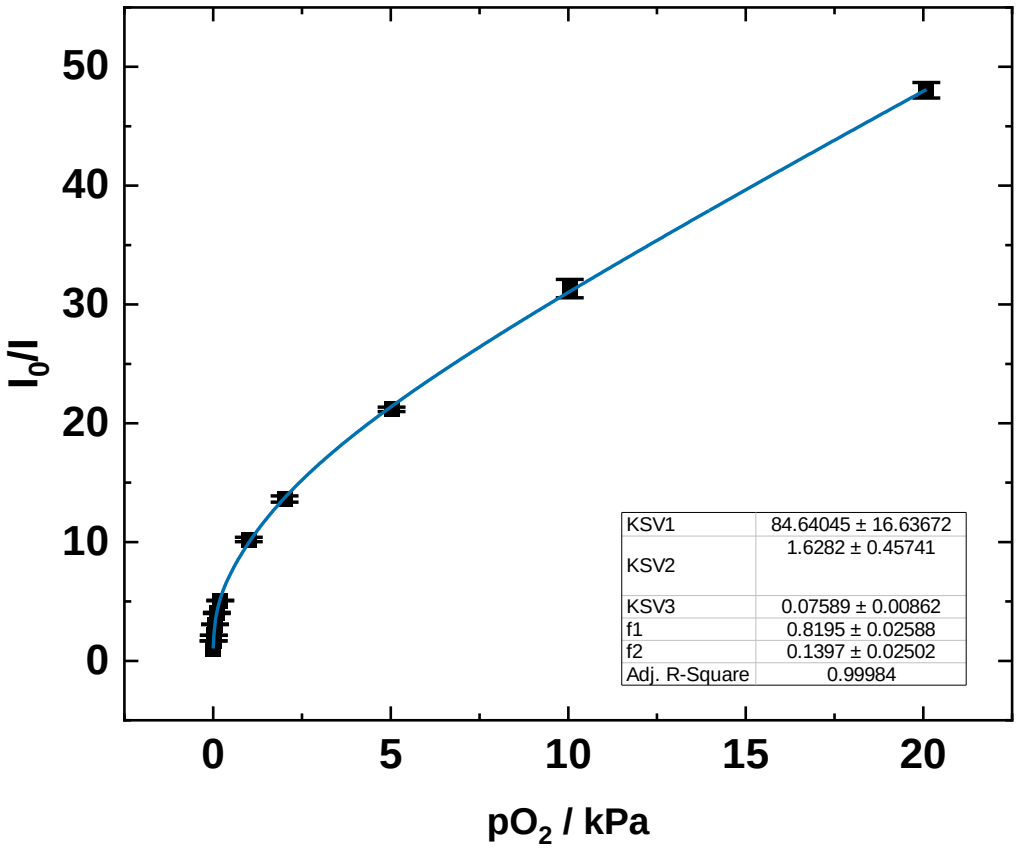

Fig. S19: Stern-Volmer plot of physically mixed MOF with a fit according to eq. S6.

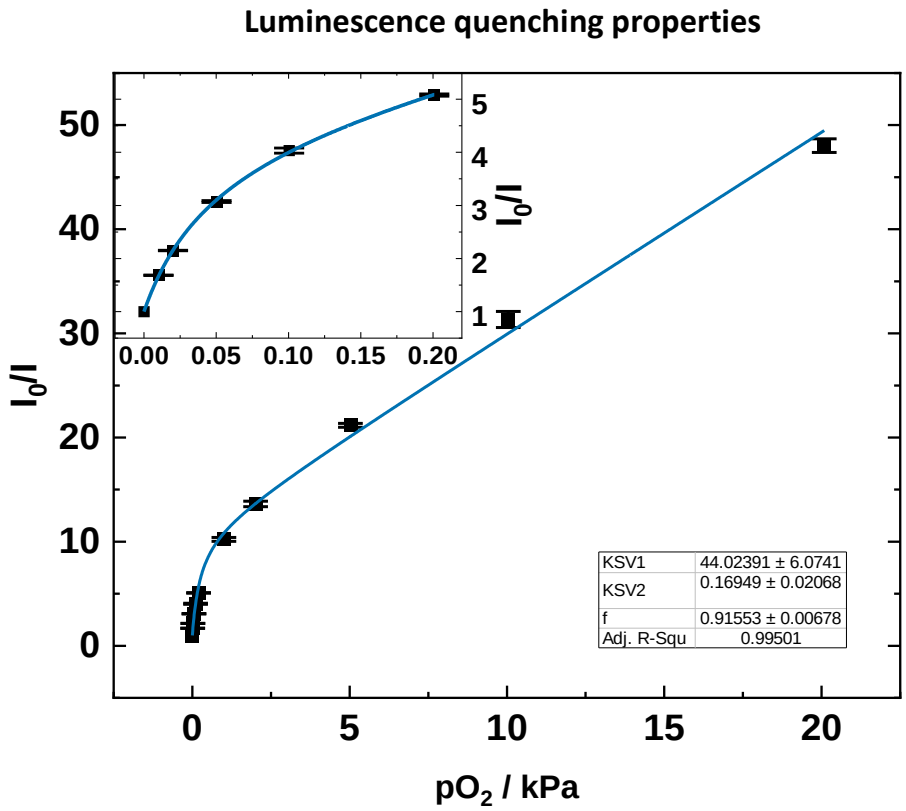

Fig. S20: Stern-Volmer plot for the physically mixed Pt(II)PCN-224 and PCN-224 MOFs. Excitation wavelength was 410 nm and the emission was recorded at 650 nm. The data are fit with eq. S2. The inset shows the calibration in trace oxygen region from 0 to 0.2 kPa pO_2. Calibrations were conducted at 23 °C.

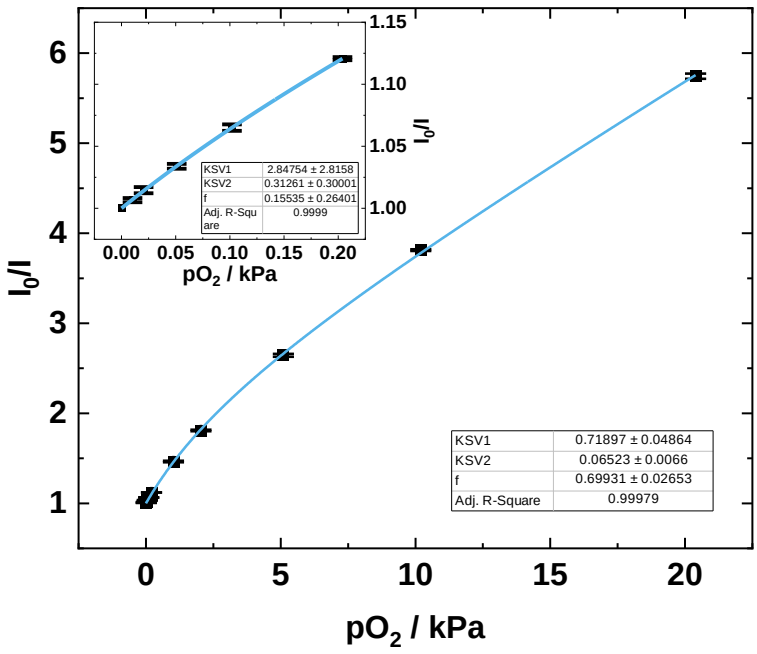

Fig. S21: Stern-Volmer plot for the statistically mixed MOF. Excitation wavelength was 410 nm and the emission was recorded at 650 nm. The data are fit with eq. S2. The insert shows the calibration from 0 to 0.2 kPa pO_2. Calibrations were conducted 23 °C.

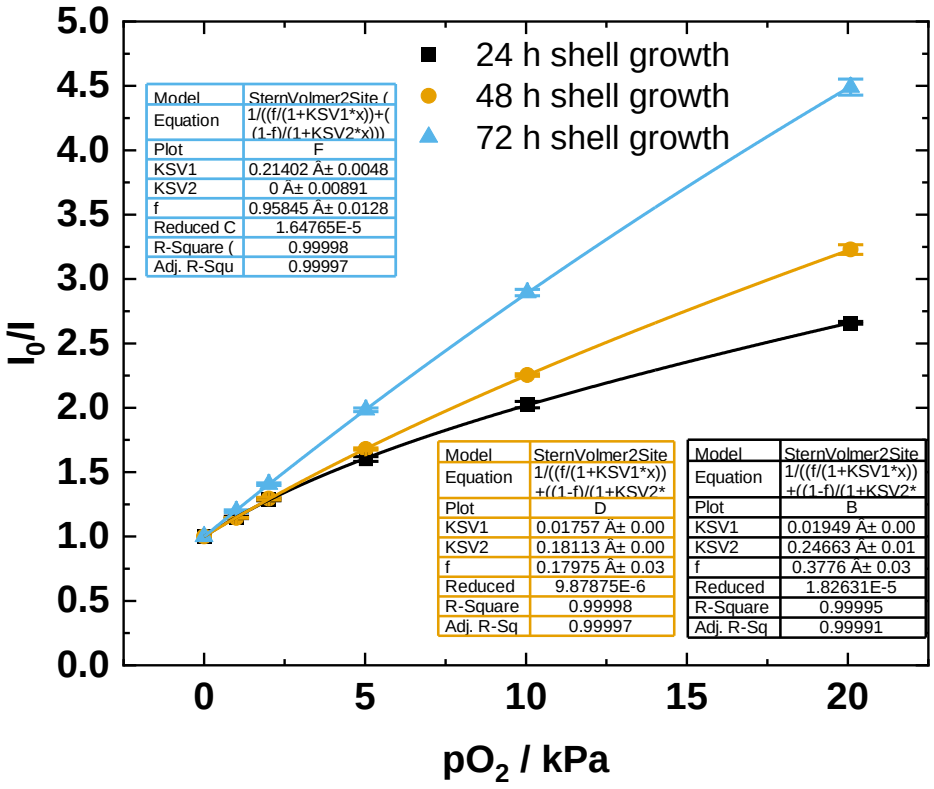

Fig. S22: Stern Volmer plots for core-shell MOF with Pt(II)PCN-224 in the core and PCN-224 in the shell after 24, 48 and 72 h of shell growth. Excitation wavelength was 410 nm. The data are fit with eq. S2. Improved linearity of the MOF after 72h shell growth can be observed. This observed increased homogeneity after 72 h shell growth agrees with the widely accepted mechanics of MOF synthesis (nucleation, growth, "healing" or error correcting [10]).

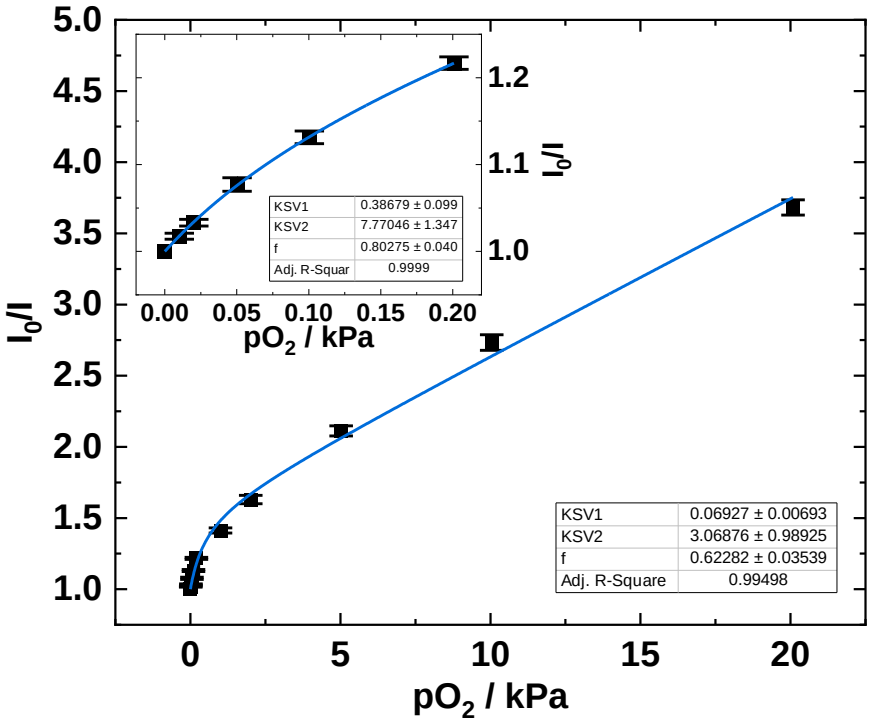

Fig. S23: Stern Volmer plots for core-shell MOF with PCN-224 in the core and Pt(II)PCN-224 in the shell. Excitation wavelength was 410 nm and emission was recorded at 650 nm. Data were fit with eq. S2.

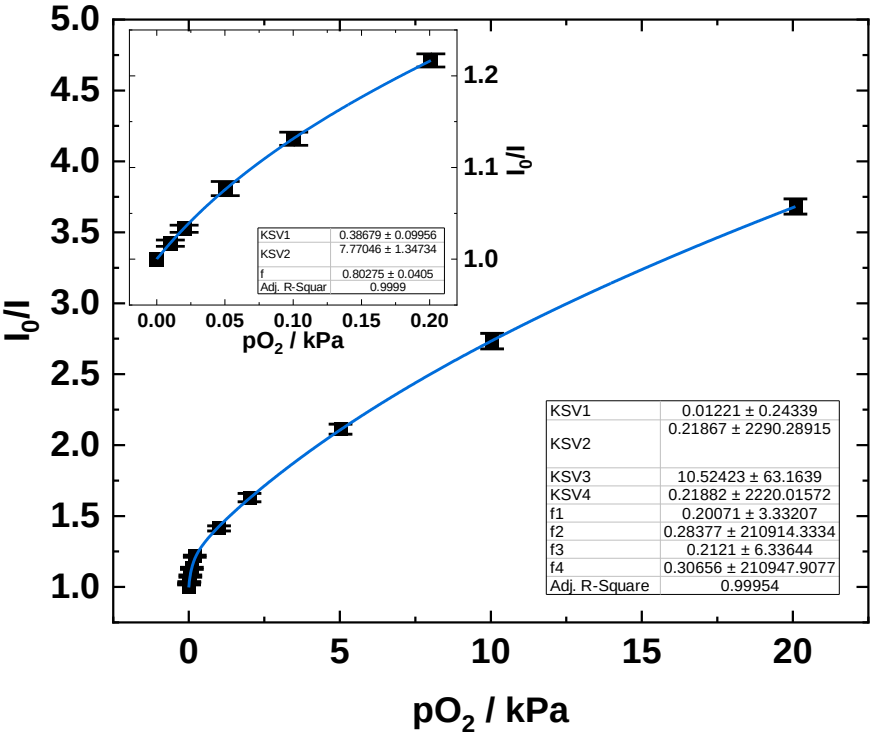

Fig. S24: Stern-Volmer plots for mixed MOF with PCN-224 in the core and Pt(II)PCN-224 in the shell. The data are identical to the those provided in Fig. S17, however eq. S2 was used to fit the Stern-Volmer plots in trace oxygen range and eq. S4 was used for the full range.

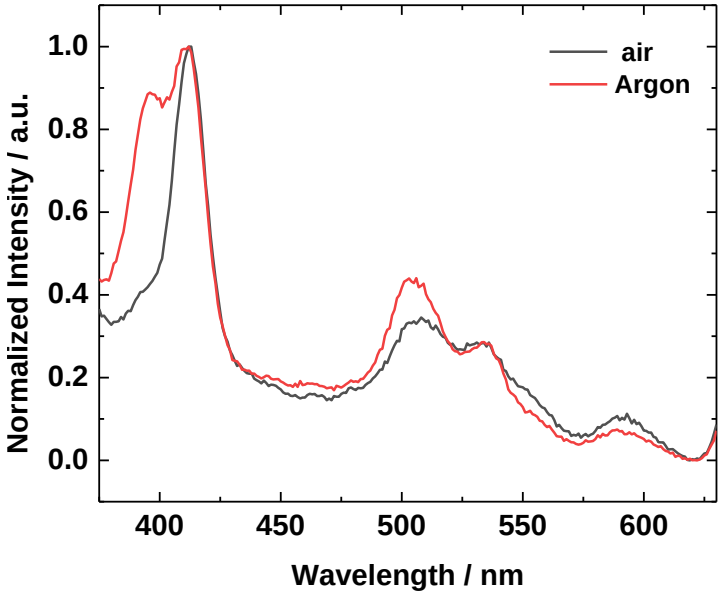

Fig. S25: Excitation spectra of physically mixed MOF in aqueous dispersion (λ_{em} 650 nm). In aqueous dispersion, the phosphorescence of the Pt(II)PCN-224 is strongly quenched in air-saturated conditions whereas the fluorescence of PCN-224 is almost not affected. Excitation spectra indicate comparable contribution of the phosphorescent MOF (Soret band at ~396 nm and 2 Q-bands in the green part of the spectrum) and fluorescent MOF (Soret band at ~412 nm and 4 Q-bands).

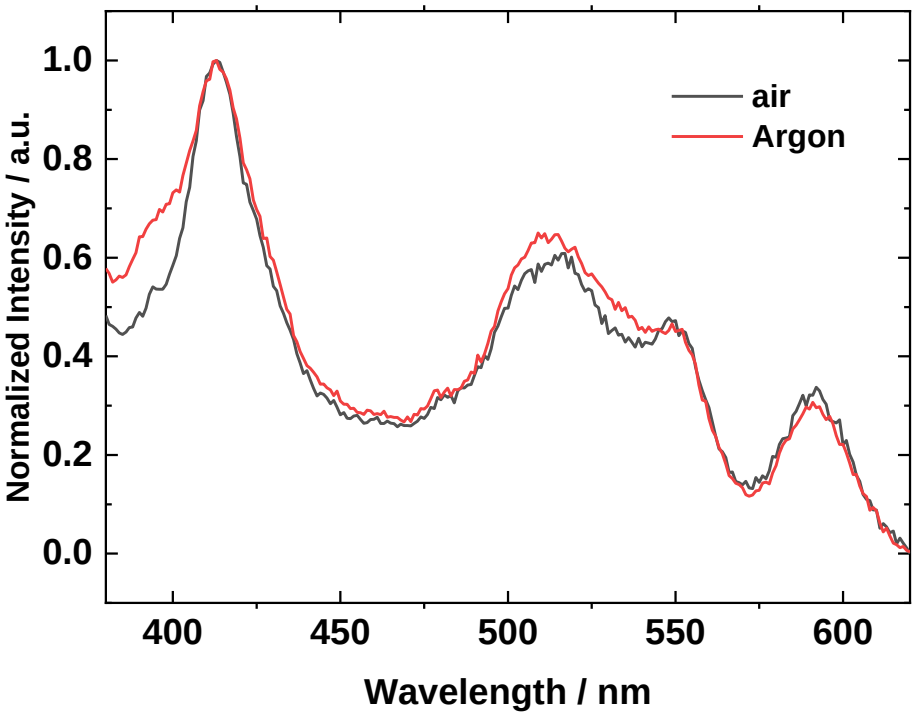

Fig. S26: Excitation spectra of statistically mixed MOF in aqueous dispersion (λ_{em} 650 nm). Excitation spectra indicate predominant contribution of the fluorescent component to the overall emission.

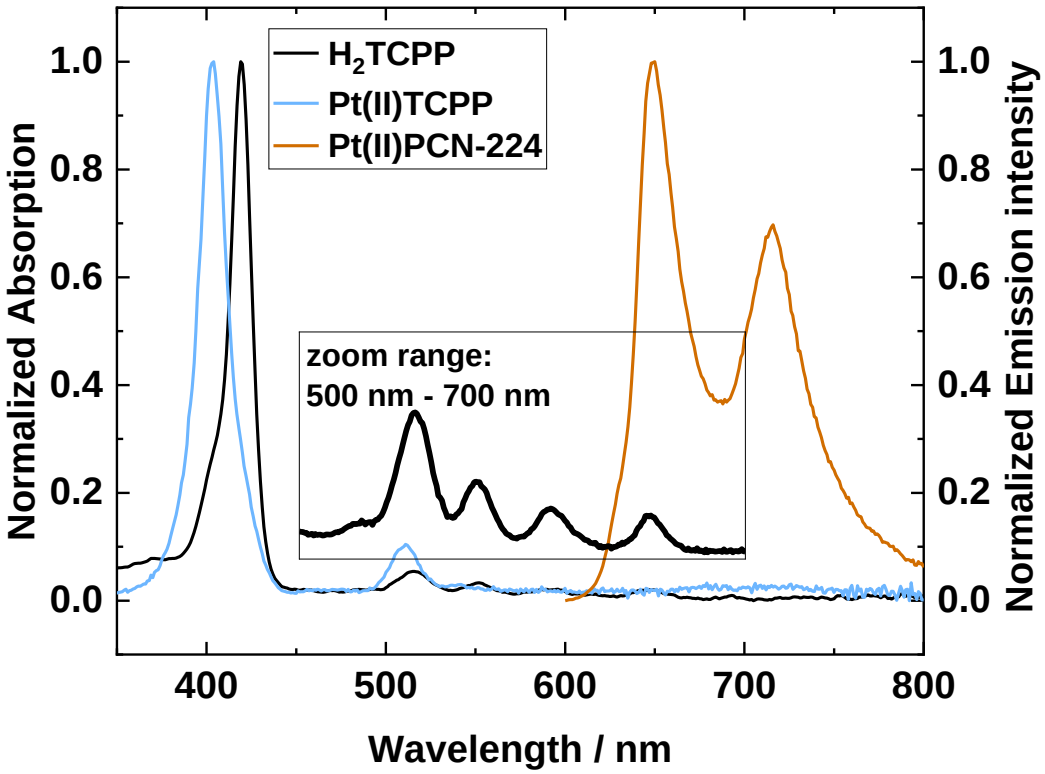

Fig. S27: Absorption spectrum (black) of H2TCPP, absorption spectrum (blue) of Pt(II)TCPP and emission spectrum (red) of Pt(II)PCN-224 MOF. Emission spectrum was recorded under nitrogen with excitation wavelength 400 nm.

The influence of the excitation wavelength on the Stern-Volmer plots for core-shell MOFs with Pt(II)PCN-224 in core and PCN-224 shell (24 h shell growth, 48 h and 72 h) and statistically mixed MOF

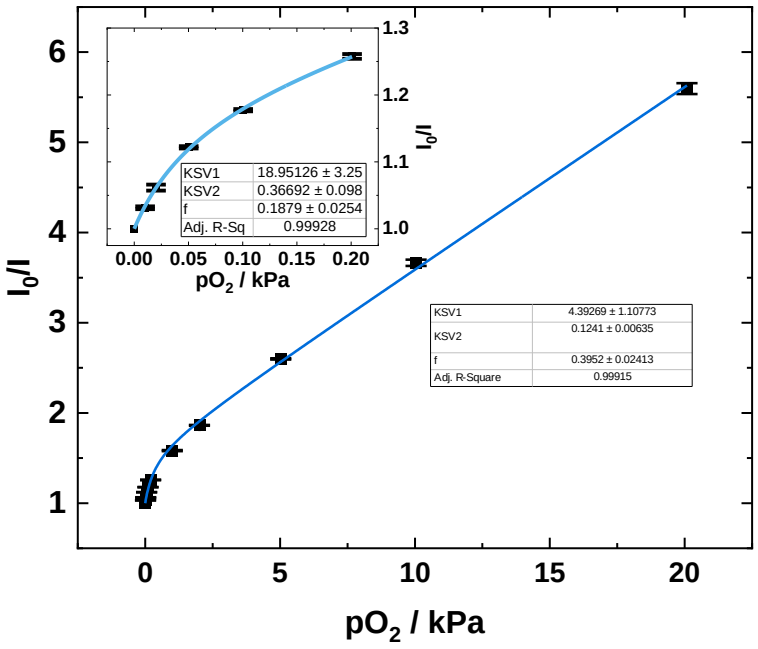

Fig. S28: Stern-Volmer plot for core-shell MOF with Pt(II)PCN-224 in the core and PCN-224 in the shell (24h shell growth) with excitation at 500 nm and detection of the emission at 650 nm. Eq. S2 was used for the fit.

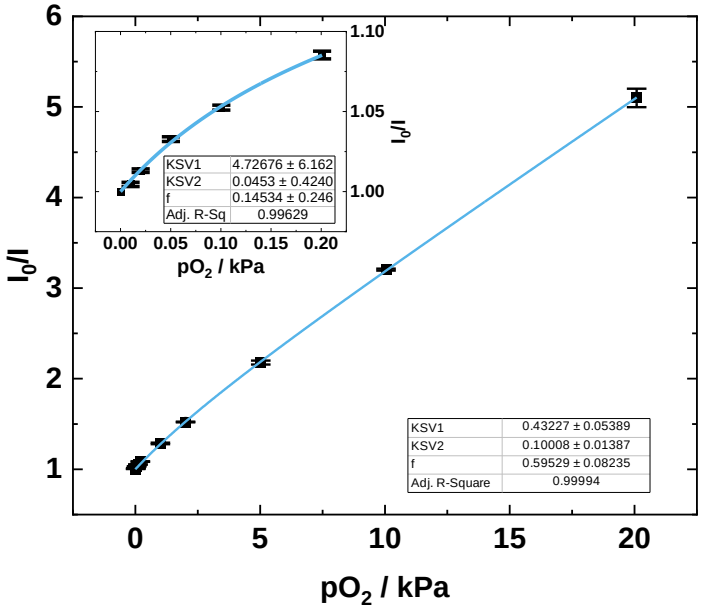

Fig. S29: Stern-Volmer plot for core-shell MOF with Pt(II)PCN-224 in the core and PCN-224 in the shell (48 h of shell growth). Excitation wavelength was 500 nm and the emission was collected at 650 nm. Data were fit with eq. S2

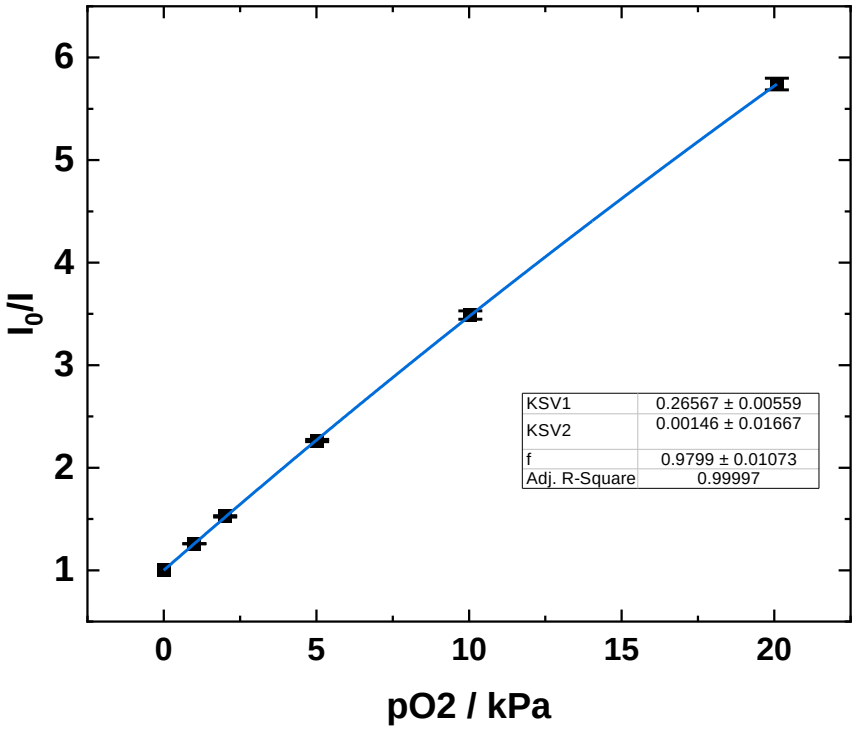

Fig. S30. Stern-Volmer plot of core-shell MOF with Pt(II)PCN-224 in the core and PCN-224 in the shell (72h shell growth). Excitation wavelength was 500 nm and the emission was collected at 650 nm. Data were fit with eq. S2.

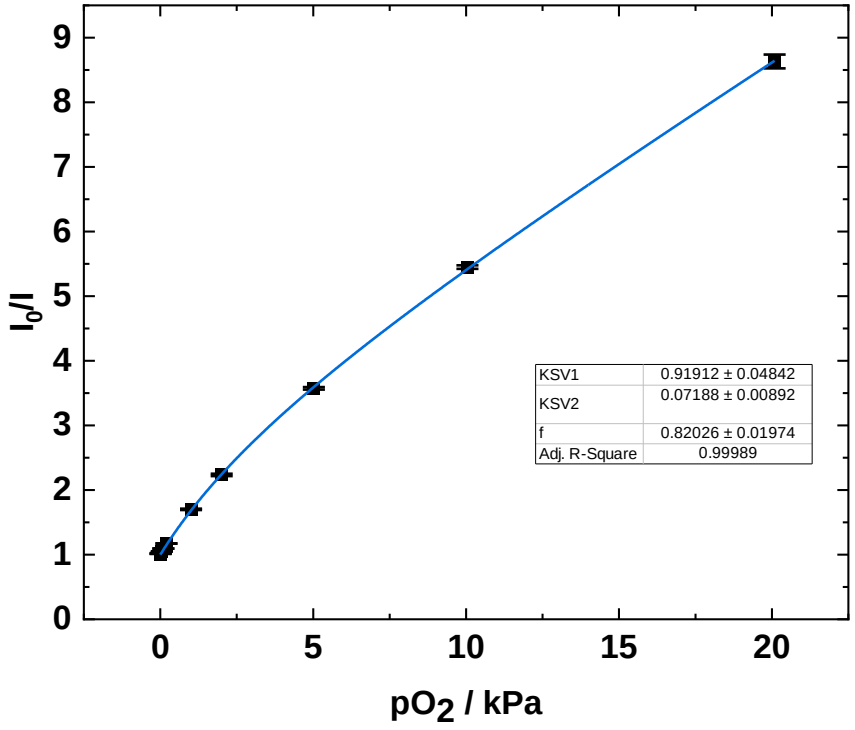

Fig. S31. Stern-Volmer plot of statistically mixed MOF obtained with excitation wavelength of 500 nm and detection of the emission at 650 nm. Data were fit with eq. S2.

Considerations regarding the impact of thickness of the shell and penetration depth of excitation light

The average edge length of the core shell materials grown with Pt(II)PCN-224 in the core and PCN-224 in the shell is around 2.6 µm after 24 h of shell growth. Excitation at different wavelengths (410 nm, 500 nm) showed that the optical filtering of excitation light influences the quenching behavior significantly.

The same experiments conducted with samples after 72 h of shell growth showed that for the thicker shells no improvement regarding sensitivity can be obtained by simply choosing a more suitable excitation wavelength. In Fig. S7 one can see that the extended shell growth leads to a second population of crystals which is significantly larger. Taking only the large crystals into consideration, the average size of these crystals is around 5.4 µm. The average size of the crystals from the second population is around 2.8 µm and not significantly different from the size of the crystals obtained after 24 h of shell growth.

Tab. S2: Size and growth of the core shell materials.

Sample	Edge length / µm	Increase of (core) +growth / µm	Increase of (24h) + growth / µm	Increase of (48h) +growth /µm
Core material	1.4			
24 h shell growth	2.6	(1.4)+ 1.2		
48 h shell growth	2.9 and 5.03	(1.4) + 1.5	(2.6) + 2.4	
72 h shell growth	2.8 and 5.4	(1.4) + 1.4	(2.6) + 2.8	2.9 + 2.5

The edge length of core-material in average is 1.4 µm. (For the following estimation, the size of the core material will be treated as constant.) After 24 h of shell growth, particles with an average size of 2.6 µm edge length are obtained. This means that a shell with a thickness of 600 nm has grown around the core-crystals from all sides (1.4µm+ 2 x 0.6µm). This shell is further increased to a thickness of 2 µm (from all sides) after 72 h of growth (1.4µm + 2x2µm).

Interestingly, the growth of the shell material within the first 24 h is slower comparing to the followed growth after 48h and 72h. This can be expected from the mixed MOFs. An onset-phase in which no consumption of organic linkers from the reaction solution takes place was also observed in kinetic experiments with statistically mixed MOF. Following that, an increase of around 2.4 µm edge length within 24 h of reaction time was found. Based on these growth rates, the estimated edge length of a pure PCN-224 (based on volume subtraction of shell/core) after 72 would be around 4-5 µm. This is in good agreement with crystal sizes frequently found with similar methods of preparation. [2]

The estimation of absorbance of PCN-224 from solution-based experiments considering the density of MOF materials results in an absorbance of around 0.5 (33 % transmission) at 418 nm for a MOF with thickness of 1 µm. Estimation was done as followed:

1. For the estimation of absorbance in the MOF, a defined amount (2.5 mg) was digested and diluted.
2. From the diluted stock solution an absorbance spectrum in a 1 mm cuvette was recorded.
3. From the density of the MOF material (available from crystallographic data), the volume of the MOF material was calculated.
4. The volume of the stock solution is known, as is the volume of the MOF and the dilution of H_2TCPP in solution compared to H_2TCPP in the MOF was calculated.

5. From the absorbance in 1 mm cuvette and dilution factor, the absorbance in a PCN-224 cube with a size of 1 µm was calculated.

The Absorbance in a cube of an optical pathway of 1 µm is around 0.5 (around 33% transmittance) with the given density of PCN-224.

The increased size of 1.2 µm edge length after 24 h of shell growth therefore corresponds to an additional optical pathway of 600 nm. That corresponds to an additional absorbance of around 0.3 (50 % transmission) and about 50% loss of the of the excitation light. Much larger crystals of 5.4 µm after 72 h (2 µm of total additional optical pathway) are expected to show about 90 % loss of excitation light (estimated absorbance of 0.96). This estimation shows the huge influence of absorbance-based inner filter effect in core-shell MOFs.

The absorbance-based inner filter effect can be minimized by excitation at 500 nm but even at this excitation wavelength significant portion of light is absorbed by thicker shells. Other effects such as i) slower oxygen transport through the thick shell to the very sensitive core material ii) extended reabsorption of emission light from the shell by a thicker core or iii) the changed ratio of Pt(II)PCN-224 to PCN-224 (1:5 after 72 h shell growth, Table 1) leading to a larger contribution of luminescence intensity from PCN-224 may contribute as well.

Absorbance in the Q-bands (514 nm) is only around 10 % compared to the absorbance in the Soret band. By excitation around the Q-band, only the absorbance of 0.05 (90 % transmittance) is expected.

Please note: the above estimations were performed for single crystals of the MOFs and are only valid if a MOF crystal monolayer is considered. In reality, a MOF powder was used which includes several layers of MOF crystals. Therefore, the optical filtering effects are expected to be much more severe than estimated here.

Pd(II)PCN-224 / Pt(II)PCN224 mixed MOFs

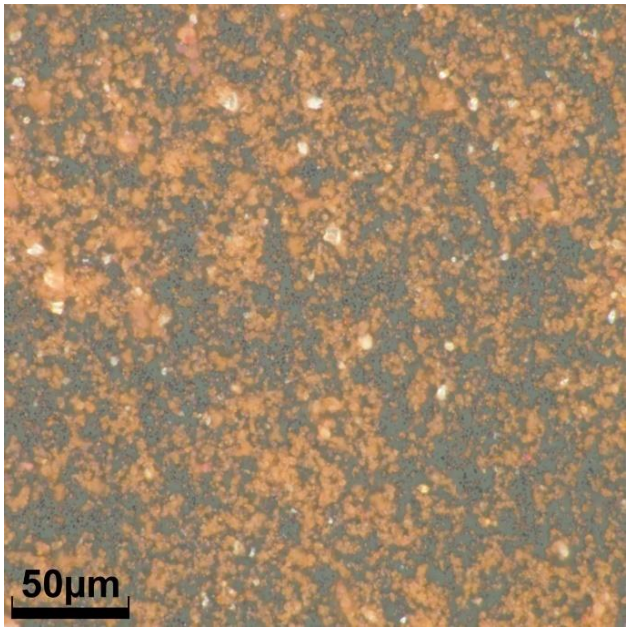

Fig. S32: Microscopic image of core-shell MOF with Pd(II)PCN-224 in the core and Pt(II)PCN-224 in the shell.

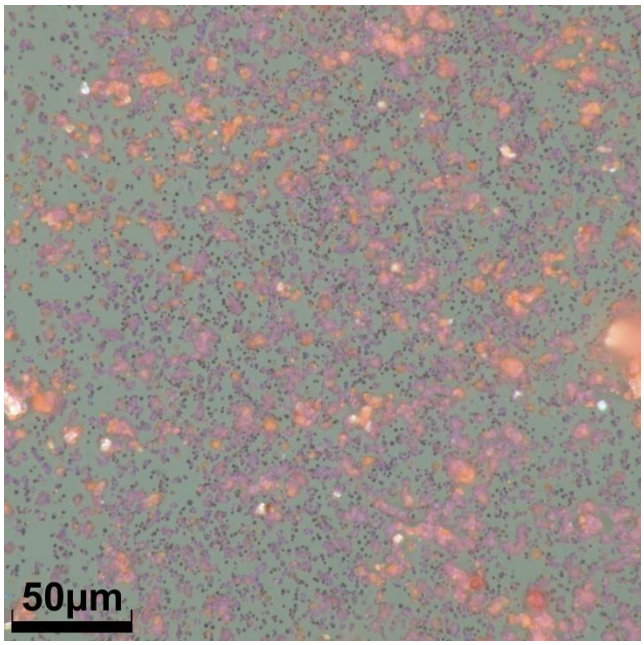

Fig. S33: Microscopic image of core-shell MOF with Pt(II)PCN-224 in the core and Pd(II)PCN-224 in the shell.

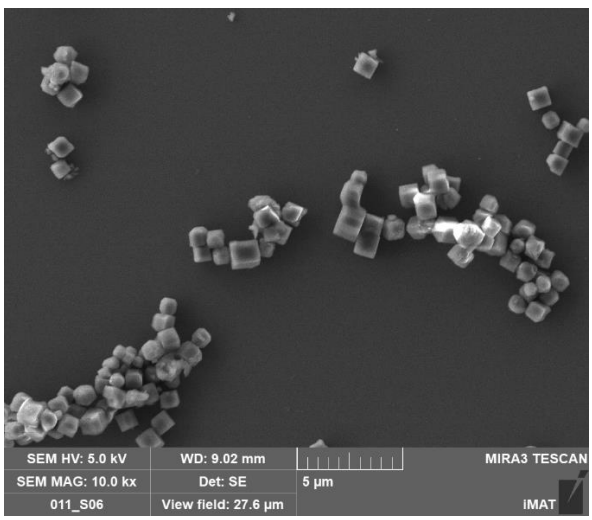

Pt(II)PCN-224 in the core and Pd(II)PCN-224 in the shell

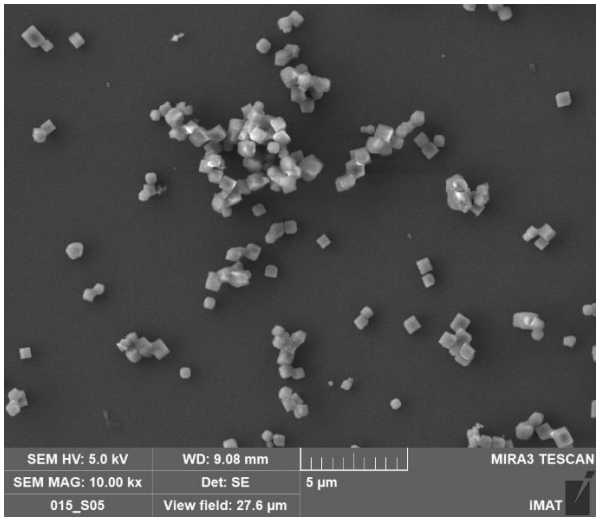

Pd(II)PCN-224 in the core and Pt(II)PCN-224 in the shell

Fig. S34: Scanning electron micrographs of mixed MOFs.

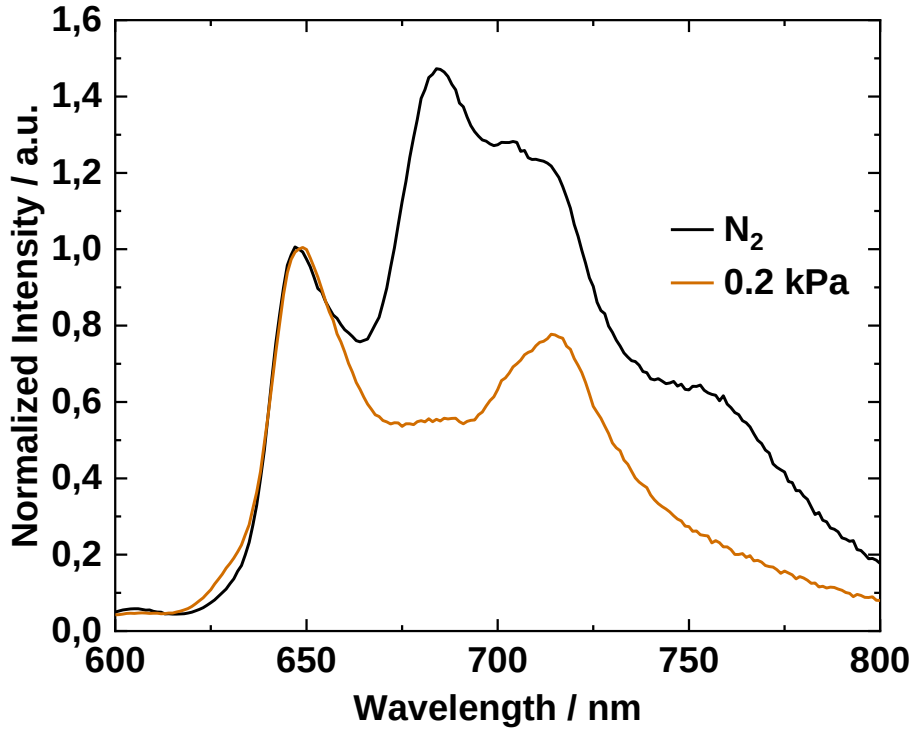

Fig. S35: Emission spectra of core/shell MOF with Pd(II)PCN-224 in the core and Pt(II)PCN-224 in the shell. Excitation wavelength was 410 nm.

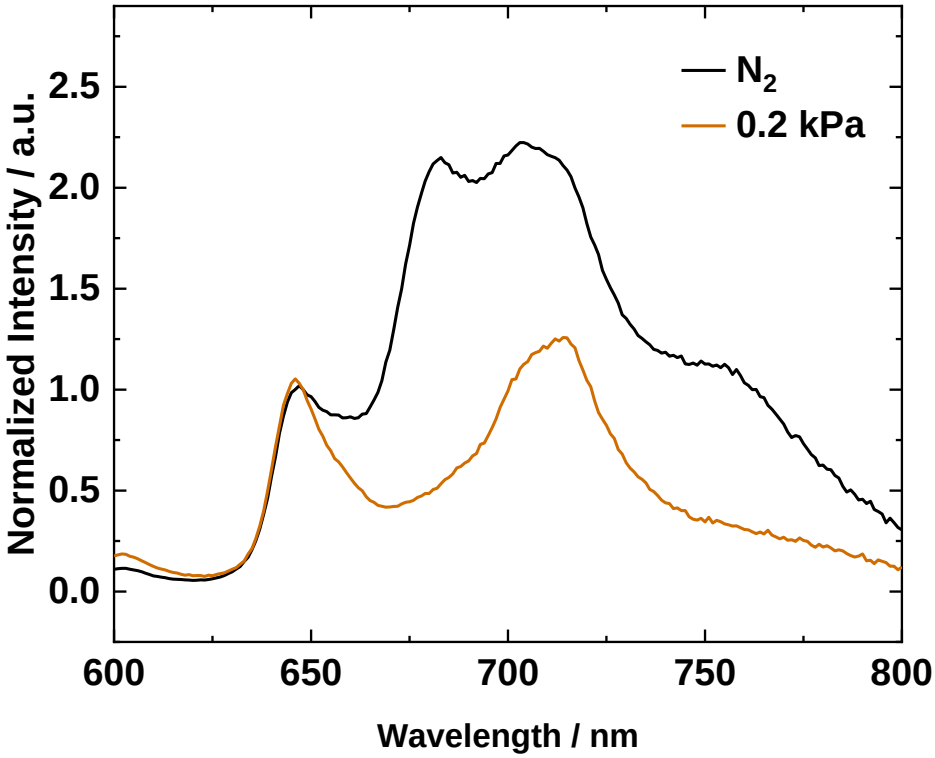

Fig. S36: Emission spectra of core/shell MOF with Pt(II)PCN-224 in the core and Pd(II)PCN-224 in the shell. Excitation wavelength was 410 nm.

References

1 M. L. Dean, J. R. Schmink, N. E. Leadbeater and C. Brückner, *Dalton Trans.*, 2008, 1341.
2 T. Burger, C. Winkler, I. Dalfen, C. Slugovc and S. M. Borisov, *J. Mater. Chem. C*, 2021, **9**, 17099–17112.
3 J. Yang, Z. Wang, Y. Li, Q. Zhuang, W. Zhao and J. Gu, *RSC Adv.*, 2016, **6**, 69807–69814.
4 J. Chu, F.-S. Ke, Y. Wang, X. Feng, W. Chen, X. Ai, H. Yang and Yuliang. Cao, *Commun. Chem.*, 2020, **3**, 5.
5 S. P. Hill, T. Dilbeck, E. Baduell and K. Hanson, *ACS Energy Lett.*, 2016, **1**, 3–8.
6 E. R. Carraway, J. N. Demas, B. A. DeGraff and J. R. Bacon, *Anal. Chem.*, 1991, **63**, 337–342.
7 H. Wu, Y. S. Chua, V. Krungleviciute, M. Tyagi, P. Chen, T. Yildirim and W. Zhou, *J. Am. Chem. Soc.*, 2013, **135**, 10525–10532.
8 A. K. Cheetham, T. D. Bennett, F.-X. Coudert and A. L. Goodwin, *Dalton Trans.*, 2016, **45**, 4113–4126.
9 T. D. Bennett, A. K. Cheetham, A. H. Fuchs and F.-X. Coudert, *Nat. Chem.*, 2017, **9**, 11–16.
10 A. Sorrenti, L. Jones, S. Sevim, X. Cao, A. J. deMello, C. Martí-Gastaldo and J. Puigmartí-Luis, *J. Am. Chem. Soc.*, 2020, **142**, 9372–9381.